4 Search for Cold Dark Matter Particles with XENON

A. Askin, L. Baudis, A. Behrens, A. Ferella, M. Haffke, A. Kish, A. Manalaysay,
T. Marrodan-Undagoitia, R. Santorelli, E. Tziaferi

in collaboration with:
Columbia, INFN, University of Coimbra, University of Münster, Rice, Subatech, Waseda

(XENON Collaboration)

The goal of XENON (1) is to search for interactions of dark matter particles in liquid xenon. Weakly Interactive Massive Particles (WIMPs) represent a generic class of dark matter candidates (2; 3). Their density in the galactic halo may allow them to be detected in laboratory experiments by looking for the nuclear recoils produced in elastic scattering of WIMPs off nuclei (4). A WIMP with a typical mass between a few GeV and 1 TeV will deposit a recoil energy below 100 keV in a terrestrial detector. The expected rates are determined by the WIMP-nucleus cross section and by their density and velocity distribution in the vicinity of the solar system (3). Direct-detection experiments are beginning to significantly constrain the WIMP-nucleon scattering cross section and, for the first time, start to probe the parameter space of 'Beyond Standard Model' particle physics models (5; 6; 8; 9). Figures 4.1 and 4.2 compare the current best limits from direct detection experiments with predictions from supersymmetry, for spin-independent and spin-dependent coupling, respectively.

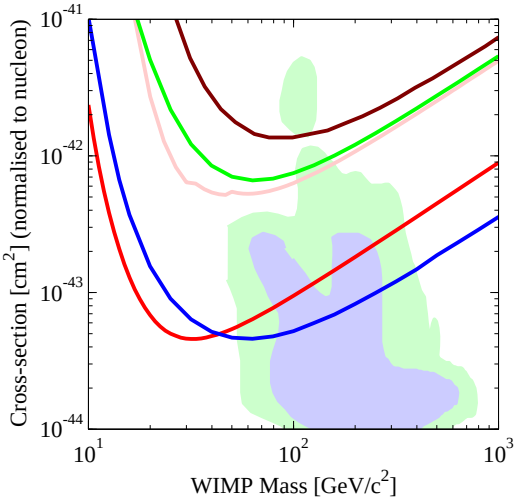

Figure 4.1: Current upper limits for the WIMP-nucleon, spin-independent, cross section as a function of the WIMP mass, the best limits being provided by the XENON10 [5] (red line) and CDMS [6] (blue line) experiments. The predicted region for the neutralino as a dark matter candidate in the constrained MSSM is shown as the green (95% CL) and blue (68% CL) shaded regions [7].

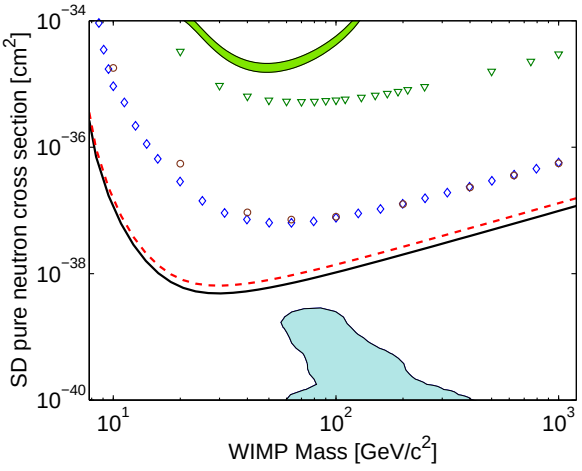

Figure 4.2:
Solid curve: XENON10 combined 90% CL exclusion limits for ^{129}Xe and ^{131}Xe for pure neutron couplings. Dashed curve: as above with alternate form factor. Diamonds: CDMS; circles: ZEPLIN-II; triangles: KIMS. Green band: DAMA evidence region for standard WIMP nuclear recoils and dark halo parameters. Blue region: prediction for the neutralino in the constrained minimal supersymmetric model. From Ref. [8].

4.1 XENON100 and its upgrade

After the successful operation of the XENON10 experiment (5; 8), the XENON Collaboration has built a 170 kg liquid xenon time projection chamber (TPC), which is currently under commissioning at the Gran Sasso Laboratory (LNGS) in an improved XENON10 shield (10). The detector uses two arrays of low radioactive, UV-sensitive photomultipliers (Hamamatsu R8520-06-Al 1" square PMTs) to detect the prompt and proportional light signals induced by particles interacting in the 70 kg sensitive xenon region. The remaining 100 kg viewed by two rings of PMTs are used as an active shield against background. The bottom array of 80 PMTs located below the cathode and fully immersed in LXe, primarily detects the prompt light signal. The 98 PMTs of the top array located in the cold gas above the liquid, detect the proportional light signal which created by the collision of extracted electrons with Xe gas phase.

While the fiducial mass of XENON100 is increased by a factor of 10 with respect to XENON10, the background is lower by a factor of $\sim$100. This is achieved by selecting ultra-low-background materials, by moving cryogenic devices and high-voltage feedthroughs outside the shield, by using the active LXe shield, by purifying the LXe from radioactive ^{85}Kr and by an improved passive shield (5 cm of ultra-pure Cu and 20 cm water, both installed by our group). Data-taking starts in 2009 and after a raw exposure of 6000 kg days the WIMP-nucleon cross sections will have been probed down to $\sim 2\times 10^{-45}$cm^2 at a 100 GeV WIMP mass.

During the accumulation of statistics with XENON100, we are planning to start construction of an upgraded detector. The goal is to further reduce the background with a cryostat made of copper and with new photodetectors, Quartz Photon Intensifying Detectors (QUPIDs) which have been developed by Hamamatsu for operation in LXe. They are made of an avalanche photo-diode kept at 0V and a photo-cathode deposited on a quartz window, kept at -10 kV. We have shown that this new photodetector has an ultra low radioactivity (see Table 4.1) and we are planning to test its single photon counting capability, as well as its quantum efficiency by operating it in LXe in our small test chamber at UZH.

The current bottom R8520 PMT array will be replaced with 19 QUPIDs. We will remove most of the activity from the stainless steel (SS) cryostat by replacing it with a low-background, oxygen free copper (OFHC) one. As the activity of the top PMTs will dominate the background, we will double the drift length from current 30 cm to 60 cm. The activity from the top cryostat assembly, made of the lowest activity SS we have identified so far, will add negligible background compared to the top PMTs. A cross-sectional view of the proposed detector mounted inside the upgraded shield is shown in Fig. 4.3.

The dark matter search with the upgraded XENON100 would start in 2011. With two years of data and a raw background rate below 4×10^{-4} events/(kg·d·keV), the upgraded XENON100 could reach a sensitivity of $\sim 2\times 10^{-46}$cm^2, which is about a factor of 100 beyond the current best limits.

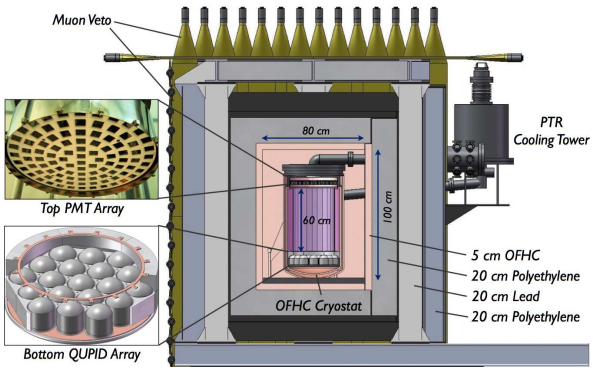

Figure 4.3: The upgraded XENON100 with 19 QUPID sensors on the bottom and an OFHC Cu cryostat in the improved shield, which includes a muon veto.

The main activities of our group are testing and calibrations of XENON100 PMTs, position reconstruction algorithms based on neural networks, material screening with the HPGe detector, Monte Carlo simulations of backgrounds and light-collection efficiencies, energy calibrations with various sources, production of the inner TPC structures, commissioning, operations, data processing and analysis, as well as R&D for the XENON100 Upgrade and XENON1t.

4.1.1 Calibration and Monitoring of the PMTs

We have the responsibility of the detailed characterization of the 242 individual PMT (Hamamatsu R8520) channels of the XENON100 detector. The light calibration involves the measurement of the absolute gain, as well as the resolution on single photoelectron, the peak-to-valley and signal-to-noise ratios, and the monitoring of the PMT responses over time. An external clock generator is used to synchronize an LED driver (which sends pulses to two InGaN/blue LEDs in an external LED box) and the data acquisition system. The light from the LEDs is transferred via an optical fiber to the feedthroughs on the detector, where it is split in order to achieve uniform illumination of all photomultiplier tubes: 4 fibers are used to calibrate top and bottom PMT arrays in the target volume, and 6 fibers for the PMTs in the veto volume. The analysis procedure identifies a PMT pulse, integrates the signal event by event, plots the spectrum for each PMT, discriminates noise and then computes the gain and other relevant parameters. A typical single photoelectron response of the PMTs being operated in XENON100 and a map of the bottom PMT array spectra is shown in Fig. 4.4. The results of the regularly performed light calibrations are written into the MySQL database, created and maintained by our group. The values are accessible by the analysis software and used for the data processing. The database also contains location and history of each phototube, quantum efficiency, gain as function of the supply voltage, and radioactive contamination from the screening.

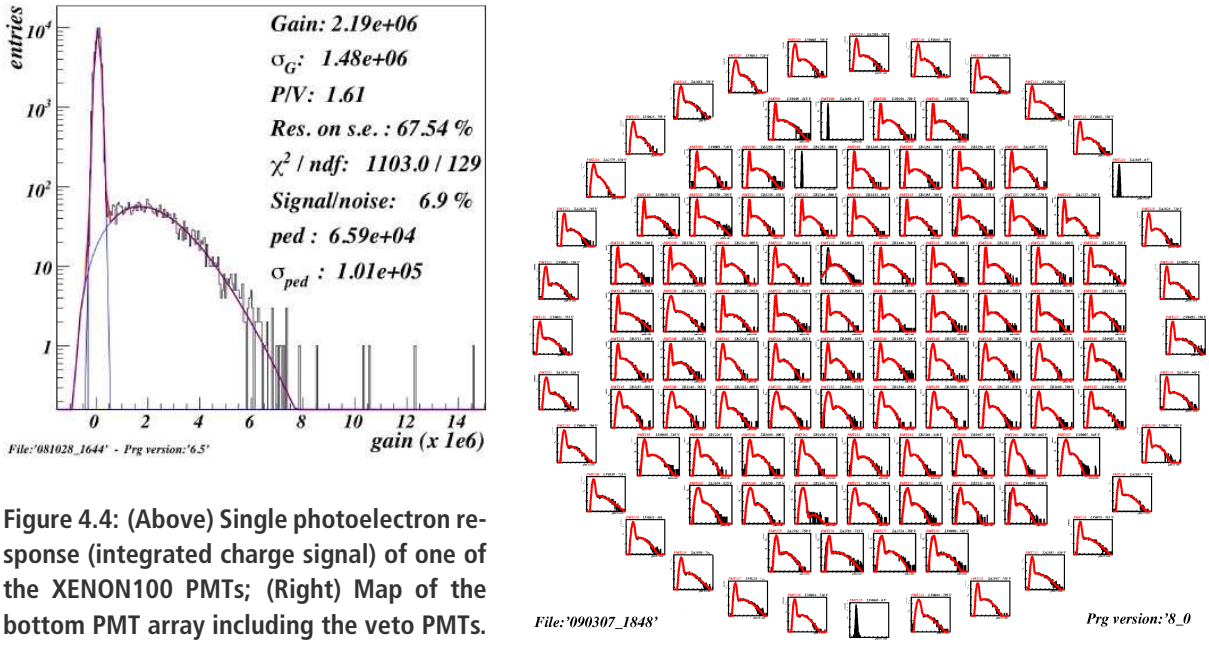

Figure 4.4: (Above) Single photoelectron response (integrated charge signal) of one of the XENON100 PMTs; (Right) Map of the bottom PMT array including the veto PMTs.

Table 4.1: **Radioactivity of XENON100 materials; average values are given if different activities were obtained for different material samples, such as different batches of PMTs and stainless steel. Upper limits are given if no activity above background was found.**

TPC Material	Unit	Quantity used	^{238}U (mBq/unit)	^{232}Th (mBq/unit)	^{40}K (mBq/unit)	^{60}Co (mBq/unit)	^{210}Pb (Bq/unit)
R8520 PMTs	PMT	242	0.15(2)	0.17(4)	9.2±1.2	1.00(8)	
PMT bases	base	242	0.16(2)	0.07(2)	$<$ 0.16	$<$ 0.01	
Stainless steel	kg	70	$<$ 1.7	$<$ 1.9	$<$ 9.0	5.5(6)	
PTFE	kg	10	$<$ 0.31	$<$ 0.16	$<$ 2.2	$<$ 0.11	
QUPID	QUPID	-	<0.49	<0.40	<2.4	<0.21	
Shield Material							
Copper	kg	1600	$<$ 0.07	$<$ 0.03	<0.06	<0.0045	
Polyethylene	kg	1600	$<$ 3.54	$<$ 2.69	$<$ 5.9	$<$ 0.9	
Inner Pb (5 cm)	kg	6300	$<$ 6.8	$<$ 3.9	$<$ 28	$<$ 0.19	17(5)
Outer Pb (15 cm)	kg	27200	$<$ 5.7	$<$ 1.6	14(6)	$<$ 1.1	516(90)

4.1.2 Material screening

We have built a low-background material screening facility at LNGS consisting of a HPGe detector in a four-layer shield of OFHC Cu and low-background Pb, placed inside a metal box including an air lock system, radon purge and a glove box for inserting the samples. The system is permanently monitored by slow control, the output of which is accessible online. We have screened all XENON100 materials, including the 242 PMTs. Apart from our own detector, we also used HPGe detectors from LNGS. Table 4.1 shows results from a subset of screened samples. We have identified low-background materials, such as the stainless steel used for the cryostat and the high-voltage grids, as well as the PTFE used for the TPC structure and PMT holder.

4.1.3 Background simulations

The screening results are used to model the gamma- and neutron-induced backgrounds caused by the natural radioactivity of detector materials and shields. For the current XENON100 the background is dominated by the PMTs, as shown in Table 4.2. For the upgraded detector, the background rate will be reduced by using QUPIDs and a Cu cryostat. Additionally, the self-shielding of LXe decreases the electron recoil (ER) rate in the central part of the target. The intrinsic ER rate due to β decays of ^{85}Kr will be reduced to 10^{-4} events/(kg d keV), with a Kr/Xe level of 5 ppt, achieved by using the cryogenic distillation column procured for the current experiment. (α, n) and spontaneous fission reactions in the detector, shielding materials, and surrounding rock/concrete are the dominant sources of neutrons. Based on the measured U/Th activities, we calculated the neutron yield using the Sources4A code (11) and simulated the nuclear recoil (NR) rates in the LXe target (Table 4.2). The dominant neutron flux comes from the rock/concrete walls of the laboratory. Since the predicted NR rate is higher than the one from the PMTs, we are currently adding 20 cm of water outside the Pb shield. The muon flux at the 3100 mwe Gran Sasso depth is 22 m^{-2}day^{-1}. We are simulating the expected background due to high-energy neutrons produced in the rock and in the shield. Preliminary estimates show that neutrons generated by muons in the shield, due to electromagnetic and hadronic showers and direct spallation, yield a total NR rate at the level of 2.7±0.7 single NRs/(100 kg·yr). To reduce this background, a

Table 4.2: **Predicted single scatter electron recoil (ER) and nuclear recoil (NR) background rates in the WIMP search region (2−12 keVee or 4.5−26.9 keVnr) in the central 50 kg (30 kg) target for the current XENON100 and in the central 100 kg target for the upgraded XENON100. To estimate the total background, the number of events and the sensitivity, we assume 99.5% ER rejection, 50% NR acceptance and 90% software efficiency.**

	Current XENON100				Upgraded XENON100	
Fiducial Mass	50 kg		30 kg		100 kg	
Background	ER	NR	ER	NR	ER	NR
Units [a]	$(10^{-3} dru_{ee})$	$(10^{-7} dru_{nr})$	$(10^{-3} dru_{ee})$	$(10^{-7} dru_{nr})$	$(10^{-3} dru_{ee})$	$(10^{-7} dru_{nr})$
PMTs and bases	4.91	3.25	<1.4	2.87	0.098	0.23
QUPIDs	–	–	–	–	<0.027	<0.10
Stainless steel	<2.01	<2.01	<0.35	<1.66	<0.052	<0.14
PTFE	<0.18	<6.99	<0.03	<5.04	<0.017	<1.60
Copper Cryostat	–	–	–	–	<0.033	<0.02
Polyethylene	<2.50	<5.37	<1.2	<4.73	<0.105	<0.60
^{85}Kr/U/Th [b]	<0.2	–	<0.2	–	<0.02	–
Concrete/Rocks[c]	–	1.34	–	1.11	–	0.2
μ-induced n in shield	–	33	–	33	–	0.7[d]
μ-induced n in rock	–	< 3.7	–	< 3.7	–	<3.7
Total Bkg	<9.8	<55.7	<3.2	<52.1	<0.35	<7.3
Run Time	40 days		200 days		600 days	
Raw Exposure	2000 kg-day		6000 kg-day		60000 kg-day	
Total Bkg events	<1.0		<1.2		<1.4	
# of WIMP events[e]	3.9		11.8		118	
SI $\sigma_{\chi-p}$ reach	6×10^{-45} cm^2		2×10^{-45} cm^2		2×10^{-46} cm^2 (2012)	

[a] dru_{ee} = evts/kg/keVee/day, dru_{nr} = evts/kg/keVnr/day
[b] with < 5 ppt Kr/Xe and U/Th in Xe below 10^{-13} g/g. The Upgrade requires another factor 10 reduction
[c] with a layer of 20 cm water outside the current shield
[d] with a 98% efficient muon veto
[e] for 100 GeV/c^2 WIMPs with spin-independent $\sigma_{\chi-p} = 10^{-44}$ cm^2

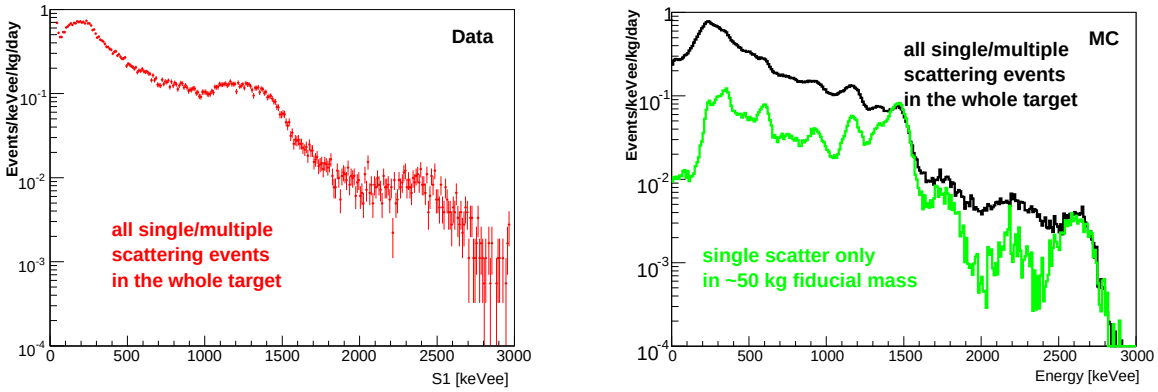

Figure 4.5: Measured (left) and MC predicted (right) background spectra in XENON100. This measurement is based on the S1 signal only, thus no position information is available.

98% efficient muon veto will be used for the upgraded XENON100. The high energy muons interacting in the rock can produce highly penetrating neutrons with energies up to few GeV, with an estimated single scatter NR rate $< 0.3/(100\,\mathrm{kg{\cdot}yr})$.

Preliminary background measurements in XENON100 have been performed with the primary scintillation (S1) signal. The measured spectrum including all event topologies (Fig. 4.5) is consistent with our Monte Carlo predictions. To obtain information on the singles rate, we need the S2 signal delivering the position information for each event.

4.2 R&D for XENON

Particles interacting in LXe produce prompt scintillation photons and ionized electrons. The *yield*, defined as the number of quanta produced per unit energy, depends on the particle species interacting in the medium. The scintillation yield of nuclear recoils relative to the scintillation yield of 122 keV gammas is known as $\mathcal{L}_{eff}$. We have recently measured $\mathcal{L}_{eff}$ at the Radiological Research Accelerator Facility (RARAF) at Columbia University. The results, shown in Fig. 4.6, tested $\mathcal{L}_{eff}$ down to 5 keV nuclear recoil energies and are not in agreement with previous data at low energies. A paper with our results and their implication for the XENON10 dark matter limits has been accepted in Phys. Rev. C (12).

The ionization yield of nuclear recoils has been measured only down to 20 keV (13). The energy threshold of XENON10 was 4.5 keV and extrapolations from higher energies were necessary. To perform new, lower energy measurements using a mono-energetic neutron beam, a dedicated dual phase xenon time projection chamber (MiniXENON) is currently being operated at the Physik Institut. A D-D neutron generator will provide the 1.5 MeV mono-energetic neutron beam. Before taking neutron data, we will test a new low-energy

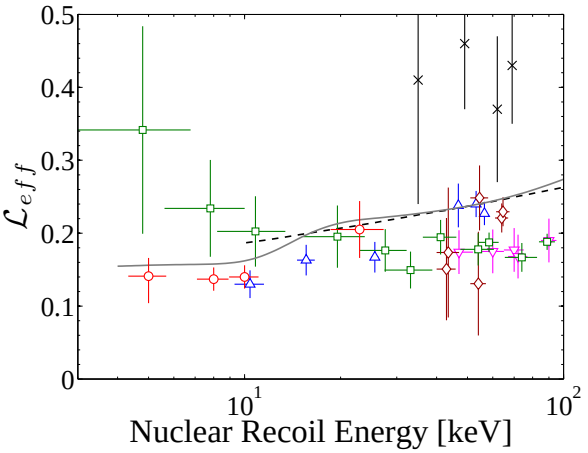

Figure 4.6: Measured $\mathcal{L}_{eff}$ values as a function of Xe nuclear recoil energy.
(○)–this work (□)–Chepel et al. [14]
(△)–Aprile et al. [15] (◊)–Akimov et al. [16]
(×)–Bernabei et al. [17] (▽)–Arneodo et al. [18]
The solid gray curve results from a recent best-fit analysis of XENON10 AmBe source data and MC [19]. Also shown is the theoretical prediction of Hitachi (dashed line) [20].

calibration source for XENON100 and the Upgrade, ^{83m}Kr. It is a decay product of ^{83}Rb, has a short half-life of 1.83 h and decays via a cascade of 32 and 9.4 keV transitions. ^{83m}Kr will be regularly introduced in the TPC, allowing S1 and S2 calibrations uniformly throughout the volume. It will also allow to determine the light and charge yield relative to low-energy gammas.

For the XENON100 Upgrade, we plan to use MiniXENON to test the new QUPID sensors. If the single photo electron response will meet our requirements, we will replace the XENON100 bottom PMT array and install an array of 19 QUPIDs. As for the current XENON100, our group will be responsible for the calibration, gain monitoring of the PMT arrays and the PMT data base.

[1] E. Aprile et al.(XENON Collaboration), New Astr. Rev. **49**, 289 (2005).

[2] B.W. Lee and S. Weinberg, Phys. Rev. Lett. **39**, 165 (1977).

[3] G. Jungman, M. Kamionkowski, and K. Griest, Phys. Rep. **267**, 195 (1996).

[4] M. W. Goodman and E. Witten, Phys. Rev. D **31**, 3059 (1985).

[5] J. Angle et al. (XENON Collaboration), Phys. Rev. Lett. **100**, 021303 (2008).

[6] Z. Ahmed et al. (CDMS Collaboration), Phys. Rev. Lett **102**, 011301 (2009).

[7] R. R. de Austri, R. Trotta, L. Roszkowski, JHEP 0707 **075** (2007).

[8] J. Angle et al. (XENON Collaboration), Phys. Rev. Lett. **101**, 091301 (2008).

[9] S. Arrenberg, L. Baudis, K. Kong, K. T. Matchev, J. Yoo, Phys. Rev. D **78**, 056002 (2008).

[10] E. Aprile and L. Baudis, Status and Sensitivity Projections for the XENON100 Dark Matter Experiment, Proceedings of Science (2009), arXiv:0902.4253.

[11] W. B. Wilson et al., SOURCES-4C: A Code for Calculating (alpha,n), Spontaneous Fission and Delayed Neutron Sources and Spectra, American Nuclei Society/Radiation Protection and Shielding Division (2002).

[12] E. Aprile, L. Baudis, B. Choi, K. L. Giboni, K. E. Lim, A. Manalaysay, M. E. Monzani, G. Plante, R. Santorelli, M. Yamashita, Phys. Rev. C **79**, 045807 (2009).

[13] E. Aprile et al., Phys. Rev. Lett. **97**, 081302 (2005).

[14] V. Chepel et al., Astropart. Phys. **26**, 58 (2006).

[15] E. Aprile et al., Phys. Rev. D **72**, 072006 (2005).

[16] D. Akimov et al., Phys. Lett. B **524**, 245 (2002).

[17] R. Bernabei et al., EPJdirect C **11**, 1 (2001).

[18] F. Arneodo et al., Nucl. Inst. and Meth. A **449**, 147 (2000).

[19] P. Sorensen et al., Nucl. Inst. and Meth. A **601**, 339 (2009).

[20] A. Hitachi, Astropart. Phys. **24**, 247 (2005).